Innovations

Surface Characterization of Quartz Materials for Enhanced Wettability in Oily Wastewater Treatment: Insights from SEM, XRD, and Raman Spectroscopy

Nthabiseng Ramanamane & Mothibeli Pita
Department of Mechanical Engineering, Bioresources and Biomedical Engineering, School of Engineering and the Built Environment, University of South Africa, Florida 1710, Private Bag X06, South Africa

Corresponding Author: **Nthabiseng Ramanamane**

Abstract: *Quartz-basedfiltration media have garnered increasing attention for oily wastewater separation due to their natural abundance, structural stability, and inherent surface reactivity. This study investigates the effects of various surface treatment processes specifically raw, washed, and nanoparticle-coated conditions on the physicochemical properties of quartz using a comprehensive multi-technique characterization approach, including Scanning Electron Microscopy (SEM), X-ray Diffraction (XRD), and Raman Spectroscopy. The results reveal significant changes in surface topography and chemical composition associated with each treatment. SEM imaging shows enhanced surface roughness following nanoparticle coating, which promotes favorable selective wettability. XRD confirms that the crystalline Si O_2 phase remains intact across all treatments, indicating preserved structural integrity. Raman spectroscopy further reveals shifts in vibrational modes, consistent with increased hydrophobic character post-coating. The application of a single-layer hydrophobic nanoparticle coating demonstrates optimal oil repellency without compromising the material's framework. These findings support the potential of engineered quartz materials as cost-effective, sustainable candidates for large-scale oily wastewater filtration systems and lay a foundation for future performance enhancements.*

Keywords: *Quartz material; Surface modification; Oily wastewater treatment; SEM; XRD; Raman spectroscopy; Wettability; Hydrophobic coating*

1. Introduction

Industrial oily wastewater presents a critical environmental challenge due to its complex composition and the persistence of oil emulsions that resist conventional treatment methods. Such wastewater originates from diverse sectors including petrochemical, mining, food processing, and automotive industries, where large volumes of oil-laden effluents are discharged daily[1]–[3]. These effluents often contain free-floating oil, dispersed oil droplets, and emulsified oil stabilized by surfactants,

making their treatment technically demanding[4]–[6]. If not properly treated, oily wastewater contributes to severe ecological damage, including soil contamination, aquatic toxicity, and disruption of natural ecosystems.

Among the emerging solutions, solid-liquid separation using mineral-based filtration media has gained momentum, with quartz material demonstrating considerable promise. Quartz (SiO_2) is a naturally abundant, chemically stable, and low-cost mineral that can be engineered to enhance surface wettability properties essential for oil-water separation[7]–[9]. Its inherent physical rigidity, thermal stability, and resistance to chemical degradation make it a durable substrate for filtration systems operating under challenging environmental conditions[10]–[12].

To facilitate efficient separation, filtration media must exhibit hydrophilic-lipophobic behaviour, enabling water to permeate while selectively repelling oil[13]–[15]. This selectivity is often achieved by tailoring surface energy and roughness. Surface engineering of quartz through physical washing and nanomaterial coatings can significantly influence these properties, thereby enhancing the separation efficiency and reducing membrane fouling[16], [17]. However, understanding how different treatments affect quartz surfaces at the microscopic and molecular levels is crucial for material optimization.

Multi-technique analytical approaches such as Scanning Electron Microscopy (SEM), X-ray Diffraction (XRD), and Raman Spectroscopy offer powerful insights into the physical and chemical transformations of quartz surfaces. SEM provides morphological data that help in evaluating surface roughness and the presence of coatings. XRD reveals structural integrity and potential phase changes, while Raman spectroscopy sheds light on molecular interactions and bonding characteristics.

This study aims to investigate the structural and morphological changes induced by various surface treatments of quartz material and their implications for wettability control. By correlating surface features with potential separation performance, the study provides a framework for material selection and surface optimization in oily wastewater filtration systems. Furthermore, the findings contribute to the development of more sustainable and economically viable filtration technologies for industrial wastewater treatment.

2. Materials and Methods

To comprehensively assess the structural and chemical modifications of quartz material for use in oily wastewater separation, a combination of material preparation techniques and advanced analytical tools was employed. This section outlines the collection, processing, and surface modification of quartz samples, followed by the application of Scanning Electron Microscopy (SEM), X-ray Diffraction (XRD), and Raman Spectroscopy to characterize the materials at both microstructural and molecular levels.

The rationale behind the selection of raw, washed, and nanoparticle-coated quartz variants lies in the need to evaluate how different levels of surface treatment influence wettability and filtration potential. Each variant was subjected to the same suite of analytical procedures to ensure consistency in data interpretation and comparative re-

liability. The integration of SEM, XRD, and Raman Spectroscopy enables a multi-faceted understanding of surface morphology, crystallinity, and chemical bonding, offering valuable insights into the material's suitability for scalable filtration systems.

These methods not only elucidate the relationship between surface structure and oil-water separation performance but also serve to validate the effectiveness of eco-friendly surface engineering strategies that preserve the bulk integrity of the quartz while enhancing its functional properties. Detailed procedures for each technique are provided in the subsequent subsections.

2.1. Sample Collection and Preparation

Raw quartz material was obtained from a natural quarry in South Africa, selected for its high silica content and relevance to industrial applications. The material was initially processed through mechanical crushing and sieving to achieve particle sizes within the range of 1–2 mm. To investigate the effect of surface treatment on the physicochemical properties of the quartz, three sample variants were prepared:

- **Raw Quartz:** Untreated and directly characterized after sieving.
- **Washed Quartz:** Subjected to a low-pressure deionized water wash to remove residual clay, fines, and organic impurities. This step aimed to simulate industrial pre-treatment processes that improve surface purity.
- **Nanoparticle-Coated Quartz:** Treated with a single layer of hydrophobic nanoparticles using a sol-gel dip-coating method. The coating solution consisted of silica-based nanoparticles dispersed in ethanol, with surface functionalization achieved using fluorosilanes. The quartz particles were immersed in the solution, withdrawn at a controlled rate, and cured at 80°C to ensure uniform adherence.

2.2. Scanning Electron Microscopy (SEM)

SEM analysis was conducted using a JEOL JSM-7600F Field Emission Scanning Electron Microscope. Each sample variant was fixed onto aluminum stubs with carbon tape and coated with a thin layer of gold to prevent charging under the electron beam. Images were captured at 5,000x and 10,000x magnification to evaluate surface morphology, roughness, and coating uniformity. SEM provided visual confirmation of nanoparticle dispersion and allowed qualitative assessment of pore exposure and surface cleanness post-washing.

2.3. X-ray Diffraction (XRD)

To assess the structural integrity and crystallinity of the quartz before and after surface treatment, XRD analysis was performed using a Bruker D8 Advance diffractometer equipped with a Cu Kα radiation source (λ = 1.5406 Å). Scans were conducted over a 2θ range of 10° to 80° at a step size of 0.02°. Diffraction patterns were compared with reference spectra from the International Centre for Diffraction Data (ICDD) database to identify any secondary phases or changes in lattice structure induced by the coating or cleaning process.

2.4. Raman Spectroscopy

Raman spectroscopy was utilized to investigate changes in molecular bonding and surface chemistry. A Renishaw in Via Raman microscope with a 532 nm laser source was used to obtain spectra from 100 to 1500 cm^{-1}. Each sample was analyzed in multiple regions to ensure reproducibility. The focus was placed on the symmetric stretching modes of Si–O–Si (~464 cm^{-1}) and other potential vibrational shifts or broadenings that could indicate surface modification or interaction with coating agents. This analysis offered insights into the chemical alterations resulting from washing and nanoparticle deposition.

Together, these methodologies provided a comprehensive understanding of how physical and chemical surface modifications influence the microstructure and chemical composition of quartz material, with implications for its performance in oily wastewater separation applications. that they will be provided during review. They must be provided prior to publication.

3. Results and Discussion

The results presented in this section offer a multi-technique analysis of the structural, morphological, and chemical modifications observed in raw, washed, and nanoparticle-coated quartz materials. These findings are critical to understanding how surface engineering impacts the wettability and potential performance of quartz-based filtration media in oily wastewater treatment.

The elemental composition of the raw quartz sample, as determined by SEM-EDS analysis, is presented in Table 1. The primary elements identified include oxygen (O) and silicon (Si), which are the fundamental constituents of quartz (SiO_2). The oxygen content ranged from 58.32% to 66.32%, with an average of 61.65% and a standard deviation of 3.47%. Similarly, the silicon content varied between 31.25% and 42.27%, averaging 37.41% with a standard deviation of 3.97%.

The presence of aluminium (Al) was also detected in trace amounts, with concentrations ranging from 0.45% to 2.43% and an average of 0.94%. This variation may be attributed to aluminosilicate impurities commonly associated with natural quartz deposits[18]–[20]. The relatively high standard deviation in Al content (0.75%) indicates heterogeneity in the raw material, suggesting localized concentrations of secondary minerals or contamination during mining or handling processes[21]–[23].

Fluorine (F) and phosphorus (P) were not detected in any of the raw quartz samples, indicating the absence of intentional surface modifications or residual processing chemicals prior to the washing or coating stages. This confirms that the raw quartz was in its unaltered state, providing a reliable baseline for assessing changes due to subsequent treatments[24], [25].

Overall, the elemental data confirm the silica-rich nature of the raw quartz material, suitable for use as a base substrate in surface engineering applications. The relatively high silicon content and minimal presence of extraneous elements are essential for ensuring chemical stability and compatibility during functionalization processes aimed at improving wettability in oily wastewater treatment.

Table 1. Elemental Composition of Raw Quartz Sample Based on SEM-EDS Analysis

	O		**F**	**Al**	**Si**	**P**
	66,32		0,00	2,43	31,25	0,00
	56,97		0,00	0,75	42,27	0,00
	63,44		0,00	0,45	36,12	0,00
	63,18		0,00	0,56	36,26	0,00
	58,32		0,00	0,51	41,17	0,00
Average	61,65		-	0,94	37,41	0,00
STD DEV	3,47		-	0,75	3,97	0,00

The Energy Dispersive Spectroscopy (EDS) spectrum of the raw quartz sample, shown in Figure 1, provides insight into the elemental composition of the material at the microscale. Prominent peaks corresponding to silicon (Si-K), oxygen (O-K), aluminium (Al-K), and carbon (C-K) were identified in the energy range of 0–3 keV, which is characteristic of naturally occurring quartz.

The dominant Si-K peak at approximately 1.74 keV confirms the high silica content of the quartz, consistent with the SEM-EDS quantitative data presented in Table 1. The intensity and sharpness of this peak suggest a crystalline SiO_2 structure, which is advantageous for applications requiring surface stability and chemical resistance, such as in membrane-based oily wastewater treatment.

The O-K peak, appearing around 0.53 keV, further supports the presence of oxygen bonded within the silica matrix. This is indicative of a stable silicon-oxygen tetrahedral structure typical of quartz. The detection of Al-K at approximately 1.49 keV, albeit at lower intensity, implies minor alumina-based inclusions or impurities, which are commonly present in naturally sourced quartz[26]–[28]. These impurities may slightly affect the surface charge or wettability, which can be optimized through post-treatment processes.

The low-intensity C-K peak near 0.28 keV is likely attributed to surface contamination from environmental exposure or residual carbon from sample handling. Notably, no peaks corresponding to fluorine (F) or phosphorus (P) were observed, supporting the interpretation that the raw quartz sample had not undergone any surface modification or chemical treatment prior to analysis.

Overall, the EDS spectrum corroborates the elemental profile obtained from the SEM-EDS quantification. The spectral data validate the material's suitability as a base substrate for further surface function alization, especially for enhancing oil-repellent or hydrophobic characteristics in water treatment applications.

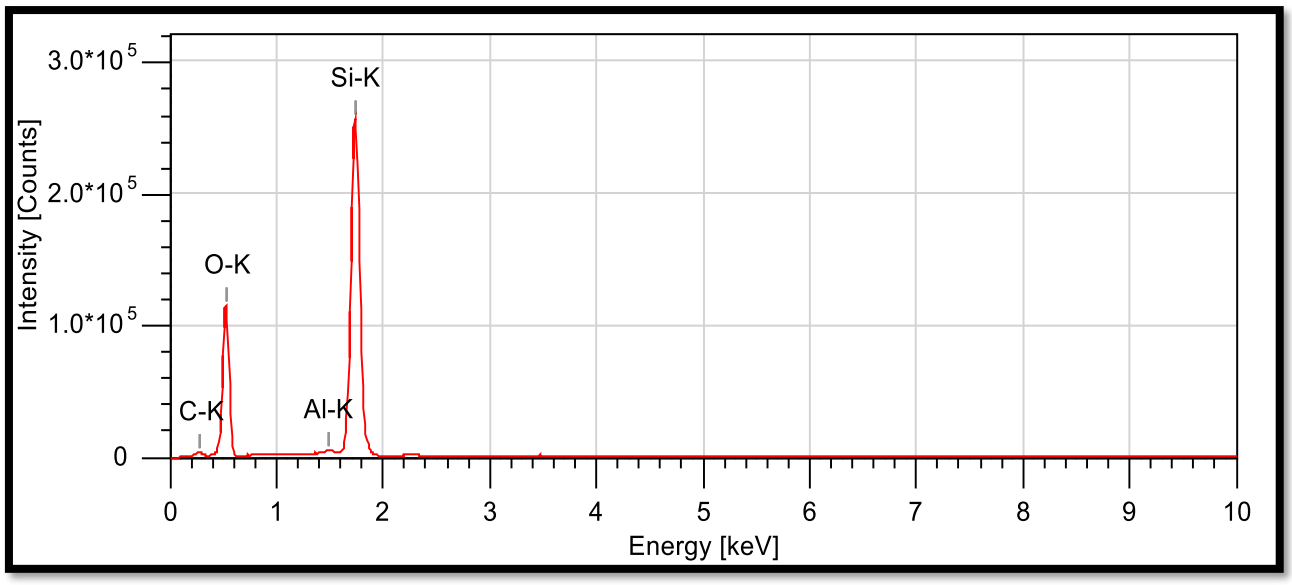

Figure 1. Energy Dispersive Spectroscopy (EDS) Spectrum of Raw Quartz Sample

The Raman spectrum of the raw quartz sample, illustrated in Figure 2, provides insight into the molecular structure and vibrational modes characteristic of crystalline silica. The most prominent peak is observed at approximately 464 cm^{-1}, which is attributed to the symmetric stretching vibration of Si–O–Si bonds within the quartz crystal lattice. This sharp and intense peak confirms the presence of highly ordered α-quartz, aligning with typical Raman signatures for naturally occurring quartz[29].

In addition to the dominant 464 cm^{-1} band, smaller peaks can be observed near 207 cm^{-1} and 355 cm^{-1}, corresponding to bending and deformation modes of Si–O bonds. The absence of broad or shifted bands in the higher wave number regions suggests minimal presence of amorphous silica or impurities such as silanols or organics. These spectral features indicate a well-crystallized and structurally stable quartz framework, which is desirable for filtration applications due to its resistance to chemical degradation and mechanical stress[30], [31].

Moreover, the lack of significant background fluorescence or noise in the range of 1000–3000 cm^{-1} further supports the high purity of the sample, as this region often reveals organic contamination or carbonaceous residues. The overall spectral clarity and peak sharpness reinforce the elemental findings from EDS, confirming that the quartz sample maintains its intrinsic crystalline properties without detectable surface alterations or lattice distortions[32], [33].

These Raman results are critical for validating the material's suitability in surface engineering strategies aimed at enhancing wettability for oil-water separation technologies. Future treatments involving surface functionalization can be benchmarked against this spectrum to assess modifications in bond vibrations and chemical interactions.

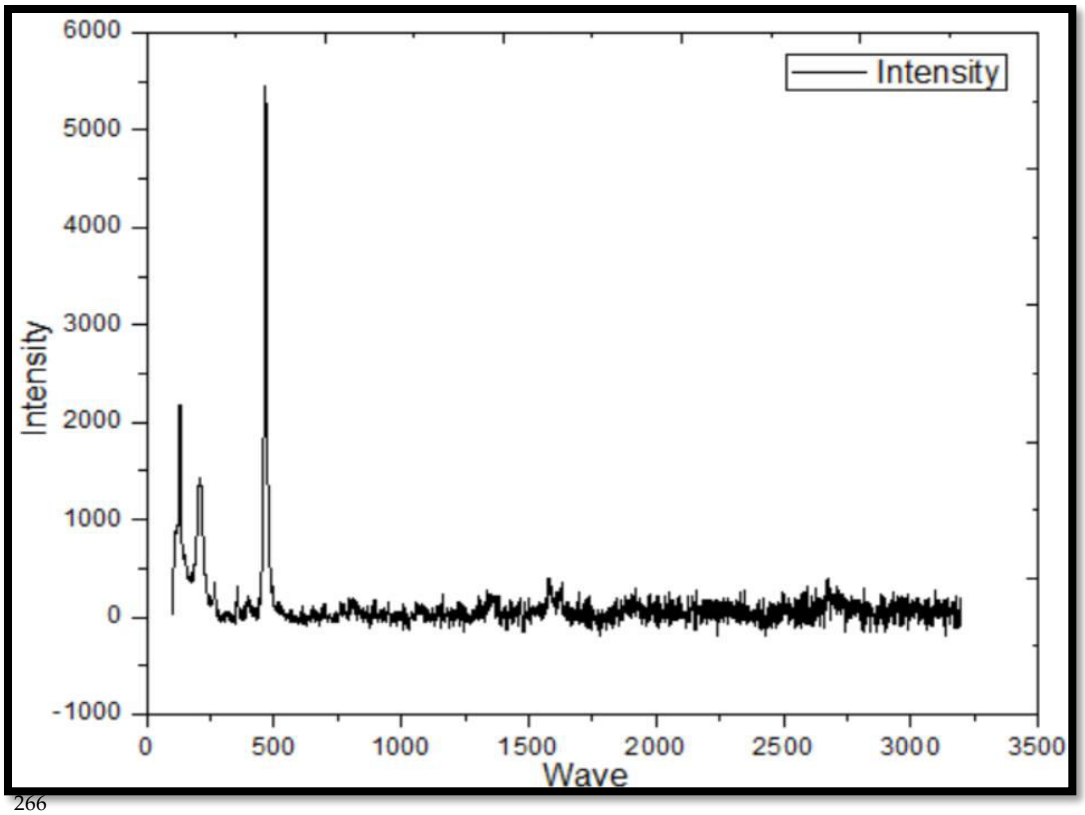

Figure 2. Raman Spectroscopy Spectrum of Raw Quartz Sample

The elemental analysis of the washed quartz sample, presented in Table 2, reveals notable shifts in chemical composition compared to the raw quartz sample (Table 1). Post-washing, the average oxygen content increased significantly to 69.82 wt%, compared to 61.65 wt% in the untreated sample. This rise in oxygen concentration is consistent with the removal of surface-bound organics and clay impurities, exposing more siloxane (Si–O–Si) linkages typical of the quartz framework.

Silicon content in the washed sample exhibited greater variability, with an average of 18.58 wt% and a standard deviation of 6.07, in contrast to the more stable 37.41 wt% average observed in the raw quartz. This decline may initially appear counter-intuitive but likely reflects a surface-level redistribution of elements due to differential etching and removal of loosely bound silica clusters[34]. In fact, localized enrichment of other surface oxides—particularly phosphorus—was also detected, suggesting leaching or surface exchange during the washing process. Phosphorus, undetectable in the raw quartz, was found at an average concentration of 11.25 wt%, indicating the adsorption or deposition of phosphate-based compounds, potentially from the washing medium or environmental exposure.

Aluminium content remained low in both cases, with the washed sample averaging 0.35 wt% versus 0.94 wt% in the raw material. This reduction supports the hypothesis that aluminosilicate clays were partially removed during the water treatment, improving surface purity[35]–[37]. The consistently absent fluorine content across both samples affirms that no fluoride-based surface modifiers were introduced.

Overall, the SEM-EDS analysis confirms that washing enhances the surface purity of the quartz by reducing clay and alumina impurities, but it also introduces chemical

heterogeneity, particularly through phosphorus enrichment. These changes may influence surface charge and wettability factors critical to oil-water separation applications. Subsequent nanoparticle coating must therefore be evaluated against this new surface chemistry to ensure uniform adhesion and optimal hydrophilic-hydrophobic balance.

Table 2. Elemental Composition of Washed Quartz Sample Obtained from SEM-EDS Analysis.

	O	**F**	**Al**	**Si**	**P**
	79,35	0,00	0,42	9,20	11,03
	64,72	0,00	0,40	25,23	9,65
	67,17	0,00	0,16	28,03	4,64
	69,50	0,00	0,42	18,59	11,49
	66,84	0,00	0,33	18,91	13,92
	66,43	0,00	0,33	17,45	15,80
	74,71	0,00	0,38	12,67	12,24
Average	69,82	-	0,35	18,58	11,25
STD DEV	4,90	-	0,08	6,07	3,28

The EDS spectrum of the washed quartz sample (Figure 3) demonstrates distinct elemental peaks corresponding to oxygen (O-Kα), carbon (C-Kα), aluminium (Al-Kα), silicon (Si-Kα), and phosphorus (P-Kα). Compared to the raw quartz spectrum (Figure 1), notable variations are evident in both intensity and elemental distribution.

The oxygen peak in the washed sample is significantly more intense than that in the raw quartz, aligning with the SEM-EDS quantitative results that reported an increase in average oxygen content from 61.65 wt% to 69.82 wt%. This enhancement suggests a cleaner quartz surface with fewer occluded impurities, leading to better exposure of the siloxane framework and potentially higher surface reactivity.

A new and prominent phosphorus peak (P-Kα) is observed in the washed sample, which was absent in the raw quartz spectrum. This supports the earlier compositional data that showed an average phosphorus content of 11.25 wt% post-washing. The presence of phosphorus could indicate the adsorption of phosphate species, possibly from environmental exposure or interaction with trace residues in the washing medium. This surface alteration may influence hydrophilicity and wettability characteristics crucial for membrane applications[38], [39].

In contrast, the intensity of the silicon peak (Si-Kα) is lower in the washed sample compared to the raw quartz. While silicon remains a major component, its apparent dilution may be attributed to either partial leaching or the masking effect of newly adsorbed species like phosphorus. This shift corroborates the compositional decrease in average Si content from 37.41 wt% to 18.58 wt%, reflecting surface chemical modification.

The aluminium peak persists in both spectra but with reduced intensity in the washed quartz, consistent with the removal of aluminosilicate impurities[40], [41]. The carbon peak remains minor, indicating minimal organic contamination—a positive outcome of the water-washing protocol.

Overall, the EDS spectral comparison confirms that washing not only purifies the quartz surface by reducing alumina and organic residues but also alters the surface chemistry through phosphorus enrichment. These changes, though beneficial for surface activation, must be carefully managed to maintain compatibility with subsequent surface function alization processes, such as nanoparticle coating.

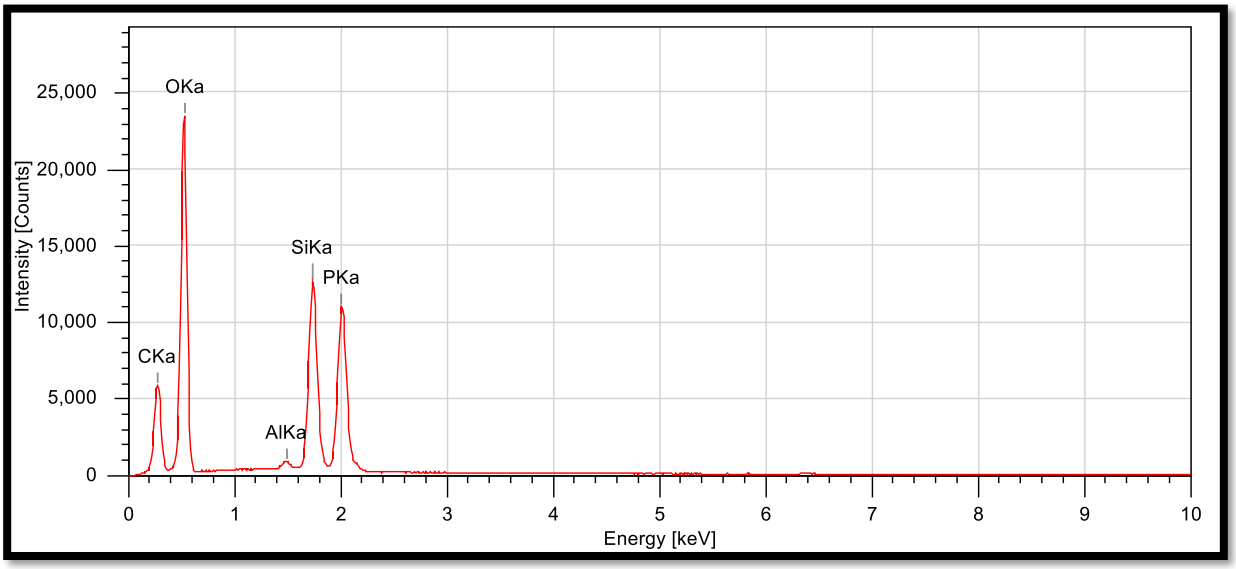

Figure 3. Energy Dispersive Spectroscopy (EDS) Spectrum of Washed Quartz Sample

The Raman spectrum of the washed quartz sample, as depicted in Figure 4, reveals several distinct vibration bands that correspond to the silica network, with enhanced signal clarity and intensity when compared to the raw quartz spectrum (Figure 2). The most prominent feature is the sharp and intense symmetric stretching band cantered around ~464 cm^{-1}, which is a characteristic signature of the Si–O–Si bond in crystalline quartz. This peak exhibits greater intensity and narrower bandwidth in the washed sample, indicative of improved structural order and reduced surface contamination.

In addition to the primary Si–O–Si peak, the washed sample also shows well-resolved lower-intensity bands in the 200–400 cm^{-1} range, which may correspond to bending vibrations within the tetrahedral SiO_4 framework. These features were less defined in the raw quartz, likely due to spectral broadening caused by the presence of amorphous phases, organic impurities, and clay minerals[42], [43].

Another significant observation is the reduced background fluorescence in the washed sample spectrum. In the raw quartz Raman profile, higher baseline noise was present, which can be attributed to residual organics and lattice defects that introduce non-crystalline scattering components. The cleaner spectrum of the washed quartz supports the successful removal of such impurities during the water-washing process[44], [45].

Minor additional bands appearing beyond 1000 cm^{-1} suggest possible surface interaction or trace contamination introduced during the washing stage, such as adsorbed phosphates, as suggested by EDS data. However, these peaks remain relatively weak and do not obscure the dominant quartz signatures.

Overall, the Raman analysis confirms that the washing process not only enhances the surface purity of the quartz material but also contributes to the preservation and amplification of its intrinsic crystalline vibrational features. The increased intensity and spectral sharpness suggest an improvement in molecular ordering and the removal of heterogeneous surface species, which is advantageous for surface modification steps such as nanoparticle coating. These spectral improvements are crucial for applications targeting enhanced wettability and surface reactivity in oily wastewater treatment systems.

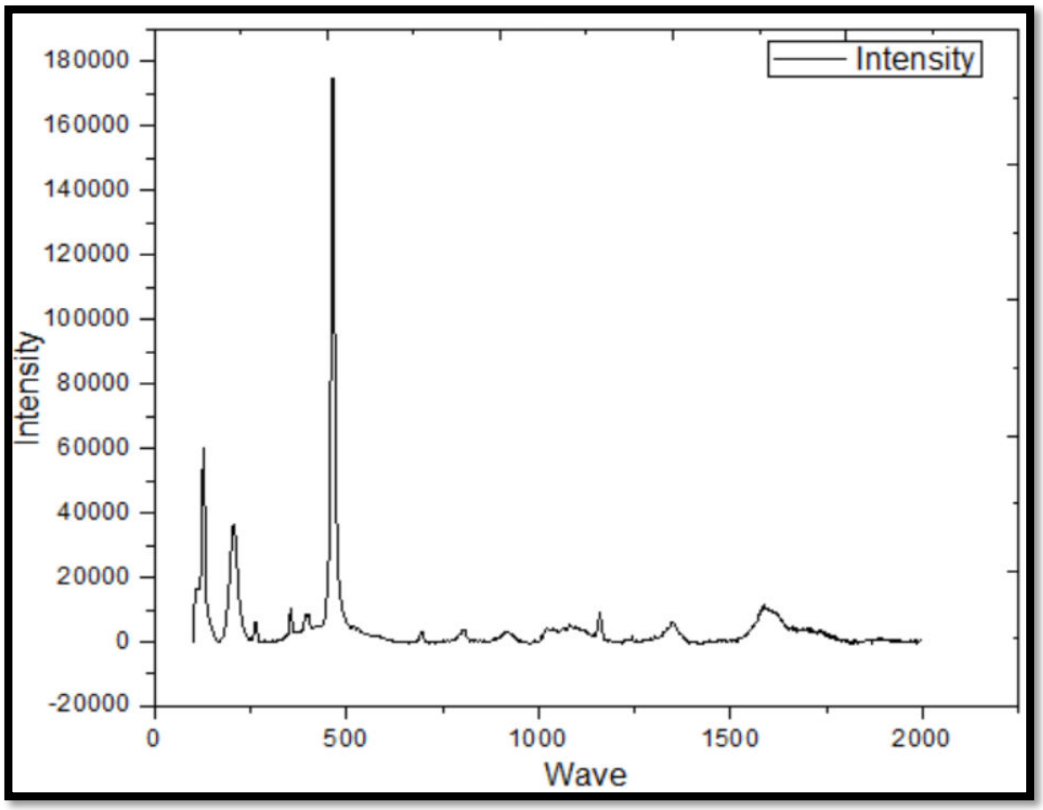

Figure 4. Raman Spectroscopy Spectrum of Washed Quartz Sample

The elemental composition of the nano particle-coated quartz sample, summarized in Table 3, reveals notable changes compared to both the raw and washed quartz materials. The silicon (Si) content averages 9.97 wt%, a substantial reduction from the 37.41 wt% observed in the raw quartz sample (Table 1). This decrease can be attributed to the surface coverage by the nano particle coating, which partially masks the underlying quartz substrate during Energy Dispersive X-ray Spectroscopy (EDS) detection. A similar trend was observed in the washed quartz sample (Table 2), although to a lesser extent, suggesting that surface modifications progressively obscure the substrate's elemental signature.

The oxygen (O) content, averaging 82.54 wt%, is significantly elevated relative to the raw sample (61.65 wt%) and the washed sample (69.82 wt%). This increase is consistent with the presence of oxygen-rich surface functional groups or bonding within the silica-based nanoparticle matrix used for coating. It may also reflect increased surface oxidation or adsorbed species introduced during the sol-gel process and subsequent curing phase.

One of the most distinguishing features in the coated quartz is the presence of fluorine (F), detected at an average concentration of 3.42 wt%. This element was absent in both raw and washed quartz samples and indicates successful surface functionalization using fluorosilane-based modifiers. Fluorinated groups are known to impart hydrophobicity and reduce surface energy—key characteristics required to enhance the performance of quartz in oil–water separation membranes[46]–[48].

Aluminium (Al) content remains relatively consistent (0.46 wt%) with that of the previous treatments, suggesting that this element is intrinsic to the quartz matrix and unaffected by the surface modifications. Conversely, phosphorus (P) is retained at a moderate level (5.89 wt%), slightly lower than that observed in the washed quartz (11.25 wt%), potentially indicating displacement or masking of adsorbed phosphate species by the coating layer.

Overall, the EDS results confirm that the sol-gel dip-coating procedure successfully introduced new surface chemistry while preserving the core material's integrity. The detection of fluorine validates the application of the hydrophobic layer, while the altered Si and O profiles support the presence of an external nanoparticle film. This modified composition is expected to significantly influence the quartz material's interfacial behaviour, enhancing its wettability performance and resistance to fouling in oily wastewater filtration applications.

Table 3. Elemental Composition of Coated Quartz Sample Obtained from SEM-EDS Analysis.

	O	**F**	**Al**	**Si**	**P**
	77,66	3,42	0,62	11,23	7,07
	85,06	0,00	0,32	9,23	5,40
	84,89	0,00	0,46	9,47	5,19
Average	82,54	3,42	0,46	9,97	5,89
STD DEV	3,45	NA	0,13	0,89	0,84

The Energy Dispersive Spectroscopy (EDS) spectrum of the nanoparticle-coated quartz sample (Figure 5) illustrates the successful incorporation of surface-modifying agents, evidenced by the presence of elemental fluorine (F-Kα) and a notable shift in the relative intensities of key peaks. Dominant peaks corresponding to oxygen (O-Kα), silicon (Si-Kα), and phosphorus (P-Kα) are observed, similar to the washed

quartz sample (Figure 3), while the appearance of a distinct fluorine signal marks the key chemical signature of the surface coating process.

Compared to the raw quartz EDS spectrum (Figure 1), which was characterized by high silicon content (~37.41 wt%) and no detectable fluorine or phosphorus, the coated sample exhibits reduced Si intensity (~9.97 wt%). This reduction likely results from surface attenuation effects caused by the applied nanoparticle layer, which partially shields the underlying silicon-rich matrix from the electron beam[49]. Concurrently, the oxygen peak has increased significantly (to ~82.54 wt%), indicating enhanced surface oxidation or hydroxylation—likely due to the silica-based nanoparticle suspension used during the sol-gel dip-coating process.

The emergence of a fluorine peak at ~0.7 keV, absent in both raw and washed quartz samples, confirms the successful deposition of fluorosilane-functionalized nanoparticles. This fluorine incorporation is critical for imparting hydrophobicity, reducing surface energy, and improving oil-repellent behaviour—key attributes in advanced water treatment materials[50]. Additionally, phosphorus content (~5.89 wt%) remains within the range observed in the washed sample, suggesting some residual influence from prior washing treatments or contributions from the nanoparticle formulation.

Aluminium content (~0.46 wt%) remains trace, consistent across all samples, indicating that surface modifications did not significantly affect the underlying aluminosilicate framework. The overall spectral profile of the coated sample, including the presence of multiple elemental peaks (C, O, F, Al, Si, P), offers robust validation of the chemical transformation of the quartz surface.

In summary, the EDS analysis of the coated quartz material demonstrates the introduction of functional chemical groups that distinguish it from its raw and washed counterparts. These changes reflect deliberate enhancements aimed at improving surface wettability and separation efficiency in oil–water treatment applications. The successful surface engineering confirmed here lays the groundwork for subsequent performance validation in membrane or packed-bed filtration systems.

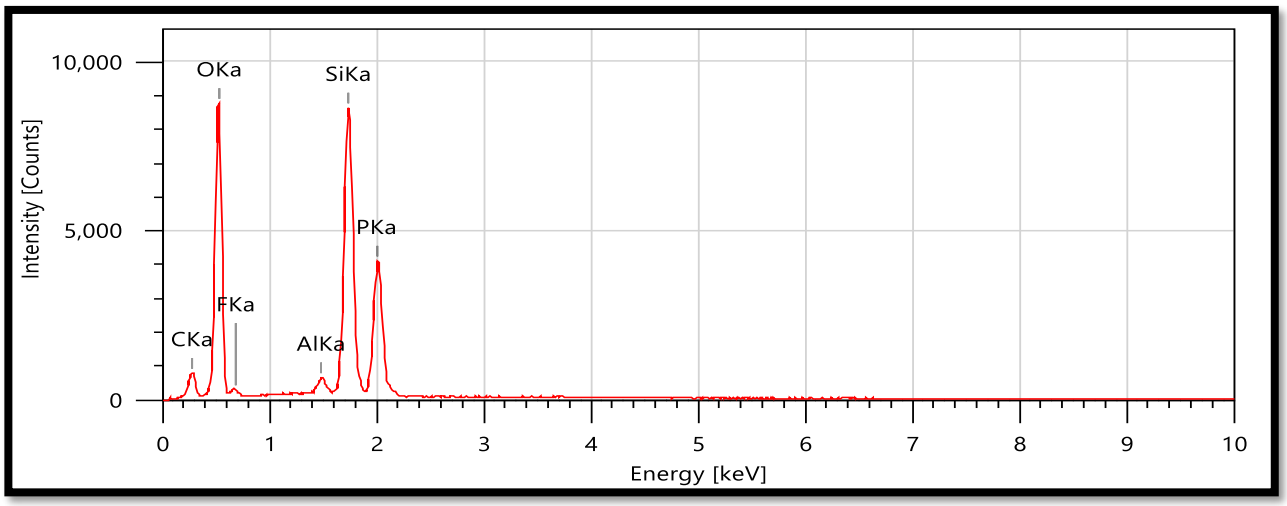

Figure 5. Energy Dispersive Spectroscopy (EDS) Spectrum of Coated Quartz Sample

The Raman spectroscopy spectrum of the nanoparticle-coated quartz sample, as illustrated in Figure 6, reveals distinct vibrational characteristics indicative of successful surface modification. The dominant peak at approximately 464 cm^{-1}, corresponding to the symmetric stretching vibration of the Si–O–Si bond, remains prominent, confirming the preserved silicate framework of the quartz substrate. However, this peak exhibits a slight broadening and intensity enhancement relative to both raw (Figure 2) and washed quartz (Figure 4), suggesting increased surface disorder and possible alteration of bond environments due to nanoparticle deposition.

Additional minor peaks observed between 200 cm^{-1} and 400 cm^{-1} are more pronounced in the coated sample, which may reflect new vibrational modes arising from interactions between the quartz surface and the silane-based coating agents. The presence of such secondary features is consistent with partial surface fluorination and silica nanoparticle adsorption, which alter local electron density and polarizability, thereby affecting Raman scattering behaviour.

Compared to the washed quartz, which exhibited sharper and more symmetric peaks with increased intensity due to the removal of impurities and better exposure of crystalline domains, the coated sample shows slightly dampened definition in the higher-frequency region (700–1300 cm^{-1}). This attenuation may be attributed to the thin nanoparticle layer overlaying the quartz surface, which scatters incident photons and reduces the signal from deeper lattice modes[51], [52]. However, the overall retention of spectral features indicates that the bulk crystallinity of the quartz remains largely intact.

Importantly, no new peaks attributable to crystalline impurities were detected, which reinforces the structural compatibility of the nanoparticle formulation with the quartz matrix. The absence of characteristic peaks from extraneous oxides or crystalline additives affirms the chemical selectivity of the surface treatment process.

The coating procedure therefore introduces subtle but meaningful modifications to the vibrational profile of quartz, consistent with partial passivation and hydrophobic functionalization[53]–[55]. These changes are significant in the context of wastewater treatment applications, as they suggest an engineered surface capable of minimizing water adhesion while resisting oil fouling—a critical property for separation media operating under multiphase flow conditions.

In conclusion, the Raman results validate the successful integration of surface-engineered functionality onto the quartz particles without compromising their fundamental silicate structure. These findings, in conjunction with SEM-EDS data, provide a multi-technique verification of the coated material's potential for enhanced oil–water separation performance.

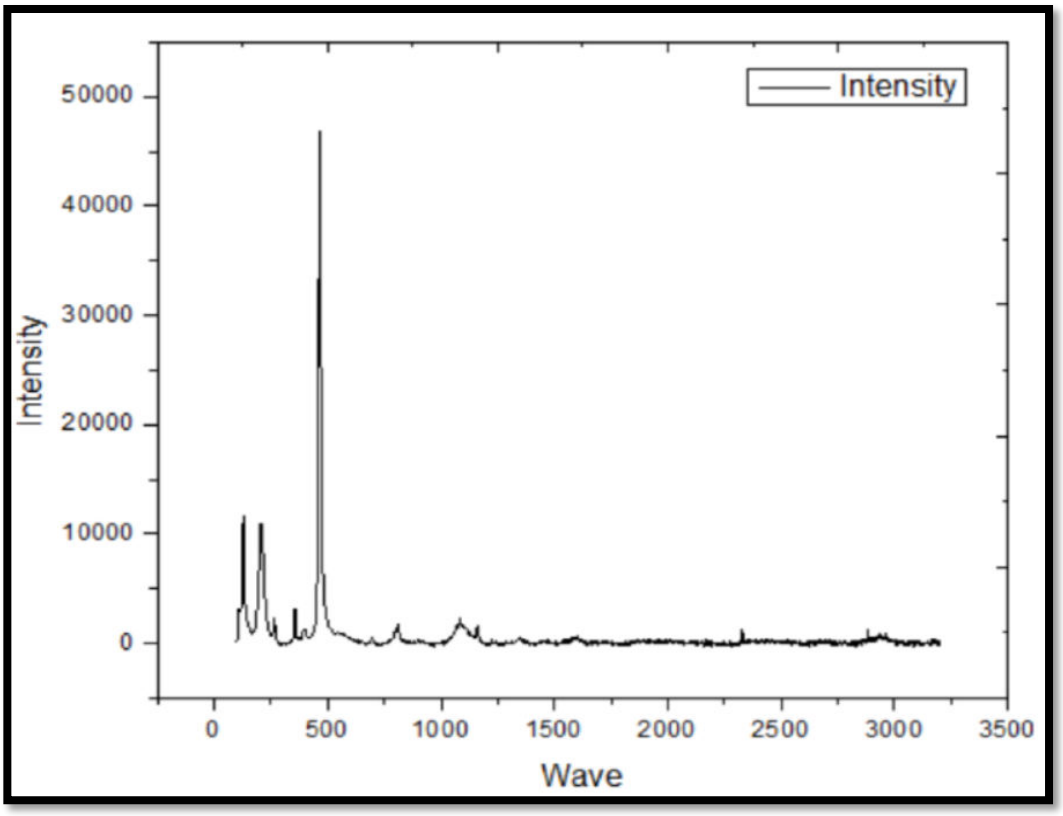

Figure 6. Raman Spectroscopy Spectrum of Coated Quartz Sample

The phase composition determined by X-ray diffraction (XRD) for raw, washed, and coated quartz samples is summarized in Table 4. This analysis provides insight into the crystalline purity and the evolution of secondary phases as a result of physical and chemical modifications.

In the raw quartz sample, a high degree of crystalline purity was observed, with SiO_2 accounting for 94.8% of the total phase content. Minor contributions from Al_2O_3 (5.2%) were detected, likely associated with alumina-based mineral impurities such as kaolinite or feldspar. No detectable phases of P_2O_5 or elemental phosphorus were found, confirming the minimal presence of phosphatic or amorphous contaminants in the untreated state.

Following washing, a notable decrease in the quartz (SiO_2) content to 87.2% was observed, accompanied by the appearance of 5.6% P_2O_5 and 2.2% elemental phosphorus (P). These findings suggest that the deionized water washing process not only reduced the alumina content marginally (from 5.2% to 5.0%) but also facilitated the surface exposure of phosphate-related phases. This could be attributed to the removal of fines and clay matrices, which may have previously obscured or masked the detection of phosphorus-bearing phases[56].

The coated quartz sample exhibited a further decline in crystalline SiO_2, reduced to 74.7%, accompanied by a substantial increase in Al_2O_3 (17.6%) and a moderate rise in P_2O_5 (7.7%). This shift is attributed to the intentional deposition of a silica–alumina nanoparticle layer via the sol-gel process, where aluminium and phosphorus-based precursors are often used to enhance adhesion and modify surface chemistry[57],

[58]. The disappearance of elemental phosphorus in the coated sample suggests either its transformation during curing or its encapsulation within the amorphous coating, rendering it undetectable by XRD.

These compositional trends align with the data observed in SEM-EDS analyses. Specifically, the coated quartz exhibited elevated Al and P contents (Table 3) consistent with the increase in Al_2O_3 and P_2O_5 phases in XRD results. Similarly, the washing stage increased oxygen content and exposed new phosphorus-containing phases that were not previously identified in the raw sample, supporting the Raman data (Figure 4) where new vibrational features emerged in the low-frequency region.

The progressive reduction in SiO_2 crystallinity from raw to coated quartz also corresponds to morphological and chemical surface changes observed via SEM and Raman spectroscopy. These changes may affect not only the surface energy and wettability of the material but also its chemical reactivity in separation processes[59], [60].

In summary, the XRD analysis confirms that the quartz modification process introduces systematic alterations in crystalline composition. These changes, particularly the enrichment of Al_2O_3 and P_2O_5 in the coated material, contribute to enhanced functionality and support its potential as a surface-engineered medium for oily wastewater separation.

Table 4. X-ray Diffraction (XRD) Data for Raw,Washed, and Coated Quartz Samples.

Sample ID	Phase matched in S-Q percentage (%)				
	SiO_2	Al_2O_3	P_2O_5	P	Total%
Raw	94.8	5.2	0.0	0.0	100
Washed	87.2	5.0	5.6	2.2	100
Coating	74.7	17.6	7.7	0.0	100

4. Conclusions

This study comprehensively examined the microstructural and chemical evolution of raw, washed, and nanoparticle-coated quartz materials using SEM-EDS, XRD, and Raman spectroscopy techniques. The findings reveal significant transformations in surface composition and crystallinity following each modification step, with direct implications for the material's applicability in oily wastewater treatment.

Raw quartz exhibited high silica purity (94.8% SiO_2) and minimal surface contamination, serving as a robust baseline. Washing with deionized water exposed phosphorus-containing phases and reduced alumina impurities, leading to enhanced surface cleanliness and a more defined Raman signal profile. The coated quartz sample demonstrated the most pronounced structural modification, characterized by reduced crystalline SiO_2 (74.7%), elevated Al_2O_3 (17.6%), and the introduction of P_2O_5 (7.7%), confirming successful nanoparticle deposition. The emergence of fluorine and the presence of sol-gel–derived elements further validate surface engineering outcomes.

Together, these results underscore the efficacy of sequential cleaning and coating treatments in tuning quartz surface properties. The modifications promote physicochemical enhancements that are crucial for improving wettability and separation efficiency in oil–water filtration systems. This work establishes a foundation for the rational design of low-cost, quartz-based materials for sustainable environmental applications.

Funding: This research was funded bythe National Research Foundation (NRF), grant number (NFSG240507217649), through the FirstRand Empowerment Foundation (FREF) under the Black Academics Advancement Programme (BAAP), as well as the University Staff Doctoral Programme (USDP) funding.

Acknowledgments: The authors gratefully acknowledge the University of South Africa (UNISA) for providing essential administrative and technical support throughout the duration of this research. The institution's research infrastructure, laboratory access, and academic environment were instrumental in facilitating the successful completion of this study.

Conflicts of Interest: The authors declare no conflict of interest.

References

- *A. Sun et al., "Design of photocatalytic self-cleaning poly (arylene ether nitrile)/nitrogen-doped Bi2O2CO3 composite membrane for emulsified oily wastewater purification," J. Environ. Chem. Eng., vol. 11, no. 5, p. 110810, 2023.*
- *T. Fan, W. Cui, Z. Yu, S. Ramakrishna, and Y. Z. Long, "Multifunctional nanofibrous membranes for highly efficient harsh environmental air filtration and oil–water separation," Appl. Surf. Sci., vol. 670, no. June, p. 160600, 2024.*
- *Z. Ren, Y. Qi, M. Zhao, B. Li, W. Jing, and X. Wei, "A composite structure pressure sensor based on quartz DETF resonator," Sensors Actuators A Phys., vol. 346, no. May, p. 113883, 2022.*
- *U. Baig et al., "Insight into soft chemometric computational learning for modelling oily-wastewater separation efficiency and permeate flux of polypyrrole-decorated ceramic-polymeric membranes," J. Chromatogr. A, vol. 1725, no. February, p. 464897, 2024.*
- *A. Felipe et al., "Recent advances in surface modification using polydopamine for the development of photocatalytic membranes for oily wastewater treatment," J. Water Process Eng., vol. 53, no. January, 2023.*
- *S. M. Abbas and S. M. Al-Jubouri, "High performance and antifouling zeolite@polyethersulfone/cellulose acetate asymmetric membrane for efficient separation of oily wastewater," J. Environ. Chem. Eng., vol. 12, no. 3, p. 112775, 2024.*
- *J. Gao, M. Qiu, X. Chen, H. Verweij, and Y. Fan, "One-step sintering for anti-fouling*

piezoelectric α-quartz and thin layer of alumina membrane," J. Memb. Sci., vol. 667, no. November 2022, p. 121188, 2023.

- *B. Peng, Y. Zhao, D. Nie, R. Yi, L. Chen, and L. Zhang, "Selective transport properties of graphene oxide membranes for various cations observed in situ using quartz crystal microbalance," Appl. Surf. Sci., vol. 541, no. September 2020, p. 148502, 2021.*
- *J. Zhao, Y. Deng, M. Dai, Y. Wu, I. Ali, and C. Peng, "Preparation of super-hydrophobic/super-oleophilic quartz sand filter for the application in oil-water separation," J. Water Process Eng., vol. 46, no. January, p. 102561, 2022.*
- *M. Manouchehri, "A comprehensive review on state-of-the-art antifouling super(wetting and anti-wetting) membranes for oily wastewater treatment," Adv. Colloid Interface Sci., vol. 323, no. December 2023, p. 103073, 2024.*
- *N. M. A. Omar et al., "Recent strategies for enhancing the performance and lifespan of low-cost ceramic membranes in water filtration and treatment processes: A review," J. Water Process Eng., vol. 62, no. May, p. 105399, 2024.*
- *A. Waheed, U. Baig, B. Abussaud, and I. H. Aljundi, "Fabrication of supported carbide-derived-carbon membrane by two phases of interfacial polymerization for oil/water separation," Ceram. Int., vol. 48, no. 6, pp. 8125–8135, 2022.*
- *J. Zhao et al., "PVDF membrane was modified by hydroxymethylated lignin to improve its hydrophilicity in treating oily wastewater," Mater. Today Commun., vol. 35, no. December 2022, p. 106055, 2023.*
- *P. Kallem, R. P. Pandey, H. M. Hegab, R. Gaur, S. W. Hasan, and F. Banat, "High-performance thin-film composite forward osmosis membranes with hydrophilic PDA@TiO2 nanocomposite substrate for the treatment of oily wastewater under PRO mode," J. Environ. Chem. Eng., vol. 10, no. 3, p. 107454, 2022.*
- *G. Kong et al., "Interfacial assembly of flexible super-hydrophilic boehmite nanofiber membranes for efficient oil-water emulsion separation," Sep. Purif. Technol., vol. 339, no. February, p. 126634, 2024.*
- *N. Ramanamane, M. Pita, and B. Sob, "Advanced Low – Cost Natural Materials for High – Performance Oil – Water Filtration Membranes : Achievements , Challenges , and Future Directions," pp. 1–22, 2024.*
- *N. Ramanamane and M. Pita, "Designing a High-Performance Oil–Water Filtration System: Surface-Enhanced Quartz with Hydrophilic Nanoparticles for Sustainable Water Reuse and Global Water Scarcity Solutions," Water, vol. 17, no. 4, p. 501, Feb. 2025.*
- *S. Radoor, J. Karayil, A. Jayakumar, and S. Siengchin, "Efficient removal of dyes, heavy metals and oil-water from wastewater using electrospun nanofiber membranes: A review," J. Water Process Eng., vol. 59, no. September 2023, p. 104983, 2024.*
- *T. J. Mabidi, O. U. Izevbekhai, W. M. Gitari, R. Mudzielwana, and W. B. Ayinde,*

"Preparation and characterization of acid-leached diatomaceous earth for application in the treatment of oily wastewater," Phys. Chem. Earth, Parts A/B/C, vol. 132, p. 103497, 2023.

- *Y. Cai et al., "Durable polyvinylpyrrolidone superhydrophilic modified ZIF-8 mesh membrane for gravitational oil-water separation and oil recovery," Colloids Surfaces A Physicochem. Eng. Asp., vol. 688, no. February, p. 133509, 2024.*
- *M. Alqassab, A. Waheed, U. Baig, S. W. Hasan, and I. H. Aljundi, "Enhancing the efficiency of polymeric-inorganic composite mixed matrix membrane for oil/water separation via SiC decoration in the polyvinyl alcohol/glutaraldehyde framework," Results Chem., vol. 7, no. January, p. 101483, 2024.*
- *P. D. Sutrisna, P. C. B. W. Mustika, R. P. Hadi, Caren, and Y. E. Gani, "Improved oily wastewater rejection and flux of hydrophobic PVDF membrane after polydopamine-polyethyleneimine co-deposition and modification," South African J. Chem. Eng., vol. 44, no. December 2022, pp. 42–50, 2023.*
- *K. Sanyal, S. Dhara, N. Gumber, and R. V. Pai, "A highly sensitive method for uranium quantification in water samples at ultra-trace level by total reflection X-ray fluorescence, after its direct pre-concentration on the surface of amidoxime functionalized quartz sample supports," Talanta, vol. 254, no. November 2022, p. 124129, 2023.*
- *Y. Liu, B. Xin, M. A. A. Newton, L. Li, and D. Huang, "Advanced photocatalytic self-cleaning membrane for highly efficient oil-water separation using C/TiO2/SiO2 composite," J. Water Process Eng., vol. 59, no. January, p. 104969, 2024.*
- *H. Osman, E. A. Said, M. Al-Bahrani, and S. Zahmatkesh, "Effect of composite membrane flux behavior on oily wastewater treatment: Predicting and optimizing based response surface methodology and AI," J. Water Process Eng., vol. 60, no. February, p. 105072, 2024.*
- *Z. Wu et al., "Photocatalytic self-cleaning membrane with polyaniline/NH2-MIL-125 heterojunction for highly oil-water/seawater separation and bacterial inactivation," Sep. Purif. Technol., vol. 323, no. April, p. 124412, 2023.*
- *H. Mao et al., "Piezoceramic membrane equipped with superwetting interface and in-situ ultrasound performance for efficient oil/water emulsion separation," Desalination, vol. 555, no. March, p. 116545, 2023.*
- *H. Mao et al., "Self-cleaning performance of in-situ ultrasound generated by quartz-based piezoelectric membrane," Sep. Purif. Technol., vol. 282, no. PB, p. 120031, 2022.*
- *J. Gao et al., "Piezoelectric porous α-quartz membrane by aqueous gel-casting with enhanced antifouling and mechanical properties," J. Eur. Ceram. Soc., vol. 43, no. 1, pp. 109–120, 2023.*

- *M. Chen, S. G. J. Heijman, and L. C. Rietveld, "State-of-the-art ceramic membranes for oily wastewater treatment: Modification and application," Membranes (Basel)., vol. 11, no. 11, 2021.*
- *E. Zhang, L. Liu, S. Jin, P. Zhao, X. Z. Wang, and G. Xu, "Preparation of corundum ceramic membrane with high permeability and corrosion resistance for oil in water separation," Ceram. Int., no. October 2024, 2025.*
- *F. U. Ahmed and D. Dhar Purkayastha, "PVDF@ZnO membrane for its potential application in oil/water separation," Mater. Today Proc., vol. 68, pp. 177–180, 2022.*
- *J. Ding et al., "A passive-active combined strategy for ultrafiltration membrane fouling control in continuous oily wastewater purification," Water Res., vol. 226, p. 119219, 2022.*
- *Y. Liu et al., "Functionalized robust-super wettability interface construction of carbon nanoparticles based on metal-based membrane and application of oil-water separation: A review," J. Water Process Eng., vol. 56, no. October, p. 104437, 2023.*
- *A. A. A. dos Santos Barbosa et al., "Low cost membrane used in oil/water removal," Desalin. Water Treat., vol. 317, no. December 2023, p. 100029, 2024.*
- *U. Baig et al., "Robust PVA/GO@MOF membrane with fast photothermal self-cleaning property for oily wastewater purification," J. Hazard. Mater., vol. 39, no. November 2023, p. 132803, Apr. 2024.*
- *M. Ağtaş, M. Dilaver, and İ. Koyuncu, "Ceramic membrane overview and applications in textile industry: A review," Water Sci. Technol., vol. 84, no. 5, pp. 1059–1078, 2021.*
- *V. S. Anggraeni, P. D. Sutrisna, P. S. Goh, E. W. C. Chan, and C. W. Wong, "Development of antifouling membrane film for treatment of oil-rich industrial waste," Mater. Today Proc., no. xxxx, Mar. 2023.*
- *P. He, F. Zhang, Y. Zhang, and H. Chen, "Multifunctional fly ash-based GO/geopolymer composite membrane for efficient oil-water separation and dye degradation," Ceram. Int., vol. 49, no. 2, pp. 1855–1864, 2023.*
- *F. Abuhatab and S. W. Hasan, "Green fabrication methods and performance evaluation of eco-friendly membranes for enhanced oil-water separation," J. Environ. Chem. Eng., vol. 12, no. 5, p. 113993, 2024.*
- *G. Zhu, X. Zhang, and Y. He, "Facile preparation of superhydrophilic and superoleophobic sand for efficient oil-water separation," J. Water Process Eng., vol. 61, no. January, p. 105355, 2024.*
- *S. Liu, F. Fan, X. Liu, Y. Guo, and Z. Ni, "Old wine and new bottles : Insights into traditional attapulgite adsorbents with functionalized modification strategies applied in efficient phosphate immobilization," J. Clean. Prod., vol. 395, no. June 2022, p. 136451, 2023.*
- *R. Wang et al., "Effects of attapulgite on the growth status of submerged macrophytes*

Vallisneria spiralis and sediment microenvironment," J. Environ. Manage., vol. 344, no. January, p. 118496, 2023.

- *P. Shi, R. Zhang, W. Pu, R. Liu, and S. Fang, "Coalescence and separation of surfactant-stabilized water-in-oil emulsion via membrane coalescer functionalized by demulsifier," J. Clean. Prod., vol. 330, no. May 2021, p. 129945, 2022.*
- *L. Wu, X. Li, F. Ye, F. Yang, and Y. Lyu, "Determination of operational parameters for the first stage of continuous temperature-phased anaerobic digestion of oily food waste : Influent concentration , hydraulic retention time , pH control and temperature," J. Clean. Prod., vol. 434, no. November 2023, p. 139960, 2024.*
- *T. Zhang, J. Zhao, D. Kong, J. Zhou, X. Wang, and B. Wei, "Solvent-responsive switching wettability of superoleophobic/superhydrophilic quartz sand filter medium facilitates rapidly oil/water separation and demulsification," Colloids Surfaces A Physicochem. Eng. Asp., vol. 697, no. May, p. 134418, 2024.*
- *Y. Li, T. Fan, W. Cui, X. Wang, S. Ramakrishna, and Y. Z. Long, "Harsh environment-tolerant and robust PTFE@ZIF-8 fibrous membrane for efficient photocatalytic organic pollutants degradation and oil/water separation," Sep. Purif. Technol., vol. 306, no. PA, p. 122586, 2023.*
- *X. Y. Han, W. X. Ma, H. R. Zhang, G. E. Chen, Y. Shi, and Z. L. Xu, "Self assembled PP membrane with photocatalytic self-cleaning performance for efficient oil/water emulsion separation," Colloids Surfaces A Physicochem. Eng. Asp., vol. 669, no. March, p. 131383, 2023.*
- *E. H. Khader et al., "Green nanoparticles blending with polyacrylonitrile ultrafiltration membrane for antifouling oily wastewater treatment," Sep. Purif. Technol., vol. 353, no. PA, p. 128256, 2025.*
- *F. Abuhantash et al., "Hydrophilic, oleophilic and switchable Janus mixed matrix membranes for oily wastewater treatment: A review," J. Water Process Eng., vol. 56, no. August, p. 104310, 2023.*
- *Y. Pan et al., "A fully degradable flexible membrane via green synthesis for highly effective separation of oil-water emulsions," Chem. Eng. J., vol. 495, no. May, p. 153319, 2024.*
- *U. Baig, M. F. Al-Kuhaili, and M. A. Dastageer, "Solar-light active tungsten oxide coated ceramic membrane with unique surface wettability fabricated by RF magnetron sputtering: Remediation of oily wastewater and photo-catalytic self-cleaning," Sustain. Mater. Technol., vol. 39, no. November 2023, p. e00837, Apr. 2024.*
- *J. Wang, L. Zhang, G. Yuan, W. She, and X. Pu, "Super-amphiphobic arabic gum-based coatings on textile for on-demand oily and dye wastewater treatment," Int. J. Biol. Macromol., vol. 251, no. August, p. 126341, 2023.*

- *C. Liu, M. Yan, K. Guo, Y. Gao, F. Liu, and B. Gao, "Ta-Fe in-situ coating PES membrane and its application in oily wastewater treatment: Insight into modification and anti-fouling mechanisms," Sep. Purif. Technol., vol. 346, no. December 2023, p. 127506, 2024.*
- *L. Cao, H. Liu, H. Li, H. Lin, and L. Li, "Journal of Water Process Engineering Dopamine co-coating with fulvic acid on PVDF membrane surface for hydrophilicity improvement and highly-efficient oily water purification," J. Water Process Eng., vol. 64, no. June, p. 105722, 2024.*
- *W. Aloulou, H. Aloulou, M. Romdhani, L. Dammak, and R. Ben Amar, "Effectiveness evaluation of a flat smectite membrane for wastewaters purification: Characterization, cost and energy estimation," Desalin. Water Treat., vol. 318, no. April, p. 100390, 2024.*
- *D. Jiang, C. Gao, L. Liu, T. Yu, Y. Li, and H. Wang, "Customized copper/cobalt-rich ferrite spinel-based construction ceramic membrane incorporating gold tailings for enhanced treatment of industrial oily emulsion wastewater," Sep. Purif. Technol., vol. 320, no. March, p. 124131, 2023.*
- *S. Basak, S. Barma, S. Majumdar, and S. Ghosh, "Role of silane grafting in the development of a superhydrophobic clay-alumina composite membrane for separation of water in oil emulsion," Ceram. Int., vol. 48, no. 18, pp. 26638–26650, 2022.*
- *U. Baig, A. Waheed, and M. A. Dastageer, "Facile fabrication of silicon carbide decorated ceramic membrane, engineered with selective surface wettability for highly efficient separation of oil-in-water emulsions," J. Environ. Chem. Eng., vol. 11, no. 2, p. 109357, 2023.*
- *K. Y. Kim, R. P. Srivastava, and D. Y. Khang, "Oleophilic to oleophobic wettability switching of isoporous through-hole membranes by surface structure control for low-voltage electrowetting-based oil-water separation," J. Memb. Sci., vol. 646, no. January, p. 120281, 2022.*